![Journal for ImmunoTherapy of Cancer]

Multiparametric MRI of early tumor response to immune checkpoint blockade in metastatic melanoma

Doreen Lau [ID],[1,2] Mary A McLean [ID],[1,2] Andrew N Priest [ID],[1,3] Andrew B Gill [ID],[1,2] Francis Scott,[1] Ilse Patterson,[3] Bruno Carmo,[3] Frank Riemer,[1] Joshua D Kaggie,[1] Amy Frary,[1] Doreen Milne,[4] Catherine Booth,[4] Arthur Lewis,[5] Michal Sulikowski,[5] Lee Brown,[5] Jean-Martin Lapointe [ID],[5] Luigi Aloj,[1,6] Martin J Graves,[1,3] Kevin M Brindle,[7] Pippa G Corrie [ID],[4] Ferdia A Gallagher [ID] [1,2]

ABSTRACT

Background Immune checkpoint inhibitors are now standard of care treatment for many cancers. Treatment failure in metastatic melanoma is often due to tumor heterogeneity, which is not easily captured by conventional CT or tumor biopsy. The aim of this prospective study was to investigate early microstructural and functional changes within melanoma metastases following immune checkpoint blockade using multiparametric MRI.

Methods Fifteen treatment-naïve metastatic melanoma patients (total 27 measurable target lesions) were imaged at baseline and following 3 and 12 weeks of treatment on immune checkpoint inhibitors using: T_2-weighted imaging, diffusion kurtosis imaging, and dynamic contrast-enhanced MRI. Treatment timepoint changes in tumor cellularity, vascularity, and heterogeneity within individual metastases were evaluated and correlated to the clinical outcome in each patient based on Response Evaluation Criteria in Solid Tumors V.1.1 at 1 year.

Results Differential tumor growth kinetics in response to immune checkpoint blockade were measured in individual metastases within the same patient, demonstrating significant intertumoral heterogeneity in some patients. Early detection of tumor cell death or cell loss measured by a significant increase in the apparent diffusivity (D_{app}) (p<0.05) was observed in both responding and pseudoprogressive lesions after 3 weeks of treatment. Tumor heterogeneity, as measured by apparent diffusional kurtosis (K_{app}), was consistently higher in the pseudoprogressive and true progressive lesions, compared with the responding lesions throughout the first 12 weeks of treatment. These preceded tumor regression and significant tumor vascularity changes (K^{trans}, v_e, and v_p) detected after 12 weeks of immunotherapy (p<0.05).

Conclusions Multiparametric MRI demonstrated potential for early detection of successful response to immune checkpoint inhibitors in metastatic melanoma.

BACKGROUND

Immune checkpoint inhibitors targeting the cytotoxic T-lymphocyte antigen-4 (CTLA-4), programmed cell death receptor-1 (PD-1) and programmed cell death receptor-1 ligand (PD-L1) are improving outcomes for increasing numbers of patients with solid cancers.[1] These drugs are now the standard of care for treating many cancers including metastatic melanoma.[2] International trials testing anti-PD-1 antibodies alone or in combination with anti-CTLA-4 antibodies in metastatic melanoma reported objective response of up to 58% and only a complete response of 11.5% at a median follow-up of 12.2–12.5 months.[3] Although durable remissions are achieved in some patients, approximately half of treated patients do not respond, while all treated patients are at risk of immune-mediated toxicity that can be both life changing and life threatening.[4][5] In clinical practice, standard CT and MRI imaging are used for evaluation of treatment response, usually undertaken at 12 weekly intervals. Assessment of response in the first few months can be difficult and can be confounded by possible pseudoprogression, characterized by the enlargement of target measurable metastases followed by subsequent regression over time. Biomarkers that could aid clinical decisions in the early stages of treatment are currently lacking.[6]

Biomarkers derived from whole blood sampling and tumor biopsy do not reflect the spatiotemporal dynamics of tumor immune response to checkpoint inhibition due to the marked interpatient, intermetastatic and intratumoral heterogeneity present in melanoma.[7][8] Pseudoprogression seen in a small number of patients receiving immune checkpoint inhibitors is difficult to distinguish from true tumor progression using size measurements alone on conventional CT.[9][10] Functional imaging techniques have the potential to longitudinally characterize individual tumor response to immunotherapy and could potentially be used in

the future to provide an early and accurate prediction of treatment response.

Several approaches have been investigated to date for imaging response to immune checkpoint inhibition. Positron emission tomography (PET) with the glucose analog 2-deoxy-2-[^{18}F]fluoro-D-glucose (^{18}F-FDG) has shown promise for long-term successful response monitoring: a complete metabolic response (CMR) with ^{18}F-FDG uptake 1 year after commencing treatment is associated with an excellent progression-free survival compared with those patients who do not show CMR.[11] However, it is not known whether ^{18}F-FDG PET can detect early response to treatment, as it can be particularly difficult to distinguish tumor metabolism from glucose uptake associated with immune infiltration after the initial introduction of immune checkpoint inhibitors.[12] Although zirconium-89 radiolabeled antibodies targeting CD8, PD-1, and PD-L1 have been developed as tracers for first-in-human trials in experimental medicine studies,[13–15] these radiolabeled approaches are expensive and cannot be easily implemented as routine clinical tools.

MRI is a widely available clinical imaging tool. The technique is particularly well suited for longitudinal tracking of early treatment response, as it does not involve exposure to ionizing radiation.[16 17] Dynamic contrast-enhanced MRI (DCE-MRI) measures properties of tissue vasculature[18] and is increasingly used in the diagnosis, staging, and treatment response assessment of many cancers.[19] Pharmacokinetic modeling of the T_1-weighted contrast-enhanced images provide quantitative measurements of tissue perfusion and vascular permeability (see online supplemental material for a detailed explanation of these parameters). For example, K^{trans} is the volume transfer coefficient from the blood plasma space into the extravascular tumor interstitial space reflecting vascular permeability, which has been shown to change following successful treatment in a number of cancer types and therapeutic regimens.[20 21] v_e is the fractional volume of the extravascular–extracellular space, and v_p is the vascular plasma volume. Following immunotherapy, DCE-MRI has been shown to detect tumor perfusion or vascular permeability as a surrogate biomarker of early tumor immune rejection in preclinical models of adoptive T cell therapy[22 23] and has been foun to distinguish pseudo-progression from true tumor progression in patients with previously irradiated melanoma brain metastases after three cycles of ipilimumab.[24]

Diffusion-weighted imaging (DWI) is a complementary approach based on the molecular movement of water in tissues, which has been widely used for probing changes in cell density due to tumor cell death that occur following successful treatment in cancer.[17 25] An advanced DWI approach termed diffusion kurtosis imaging (DKI) has been shown to detect tumor cellularity and heterogeneity in many cancer types based on the non-Gaussian movement of water within the heterogeneous tumor microenvironment.[26 27] Cell density can be quantified on DKI based on the apparent diffusivity of water (D_{app}), and

the microscopic heterogeneity of this water diffusion in tissue can be probed using a dimensionless metric termed apparent diffusion kurtosis (K_{app}). A more detailed explanation of these parameters can be found in online supplemental material.[27 28]

Here, we have used a multiparametric imaging approach combining morphological volumetric measurements with DCE and DKI to phenotype the microstructural and functional changes that occur in melanoma metastases before, during, and after treatment with immune checkpoint inhibitors.

In this prospective study, early changes in the growth kinetics, cellularity, heterogeneity and vascularity of the tumor microenvironment following immune checkpoint blockade between patients and between intermetastatic lesions were evaluated using multiparametric MRI (mpMRI). Metastatic melanoma offers a paradigm model to test the feasibility of these imaging methods in patients undergoing cancer immunotherapy.

METHODS
Study design

Patients were recruited for mpMRI as part of the MelResist study, which evaluated response and resistance biomarkers in metastatic melanoma patients undergoing systemic therapy. Written informed consent was obtained from all patients before enrolment. Patient eligibility criteria for undertaking MRI included: (A) clinical diagnosis of unresectable and previously untreated metastatic melanoma (American Joint Committee on Cancer Stage IV); (B) a treatment plan to commence standard immune checkpoint inhibitors as first-line therapy for unresectable metastatic melanoma; (C) Eastern Cooperative Oncology Group performance status score of 0 or 1 and life expectancy of 12 weeks or greater; (D) measurable disease on baseline CT (tumor diameter >1 cm); (E) availability of recent excised or biopsied tissue samples from metastatic tumors for histopathological confirmation; (F) known BRAF V600 mutation status; and (G) no contraindication to undertaking MRI.

Enrolled patients received one of the following regimens: (A) anti-PD-1 monotherapy, 2 mg/kg or 200 mg flat dose of pembrolizumab (Keytruda) every 3 weeks; or 3 mg/kg or 240 mg of nivolumab (Opdivo) every 2 weeks or 480 mg every 4 weeks and (B) combined anti-CTLA-4 and anti-PD-1 therapy, 3 mg/kg of ipilimumab (Yervoy) plus 1 mg/kg of nivolumab (Opdivo) every 3 weeks for four cycles followed by nivolumab 240 mg every 2 weeks or 480 mg every 4 weeks. All treatments were administered by intravenous infusion. Treatment continued until disease progression (as defined by the 3 monthly restaging CT scans), development of unacceptable adverse side effects such as autoimmune disorders or patient withdrawal of consent. A schematic diagram for the mpMRI study flow chart and the clinical characteristics of the study participants are as shown in figure 1 and

A
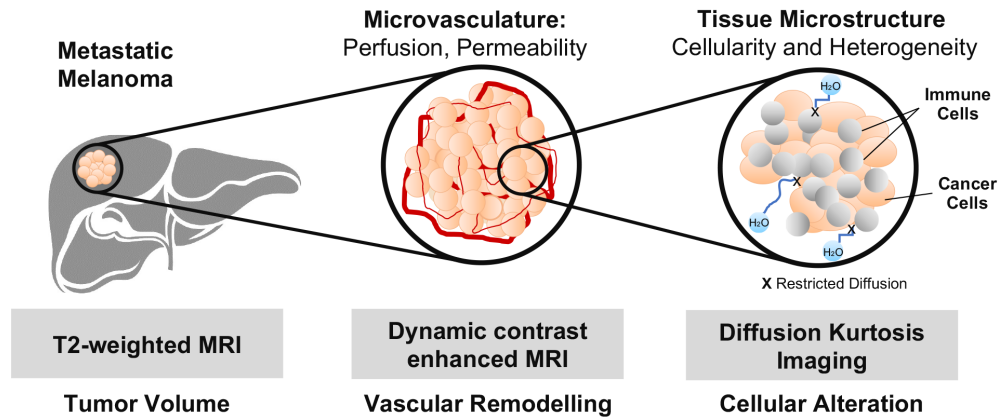
B
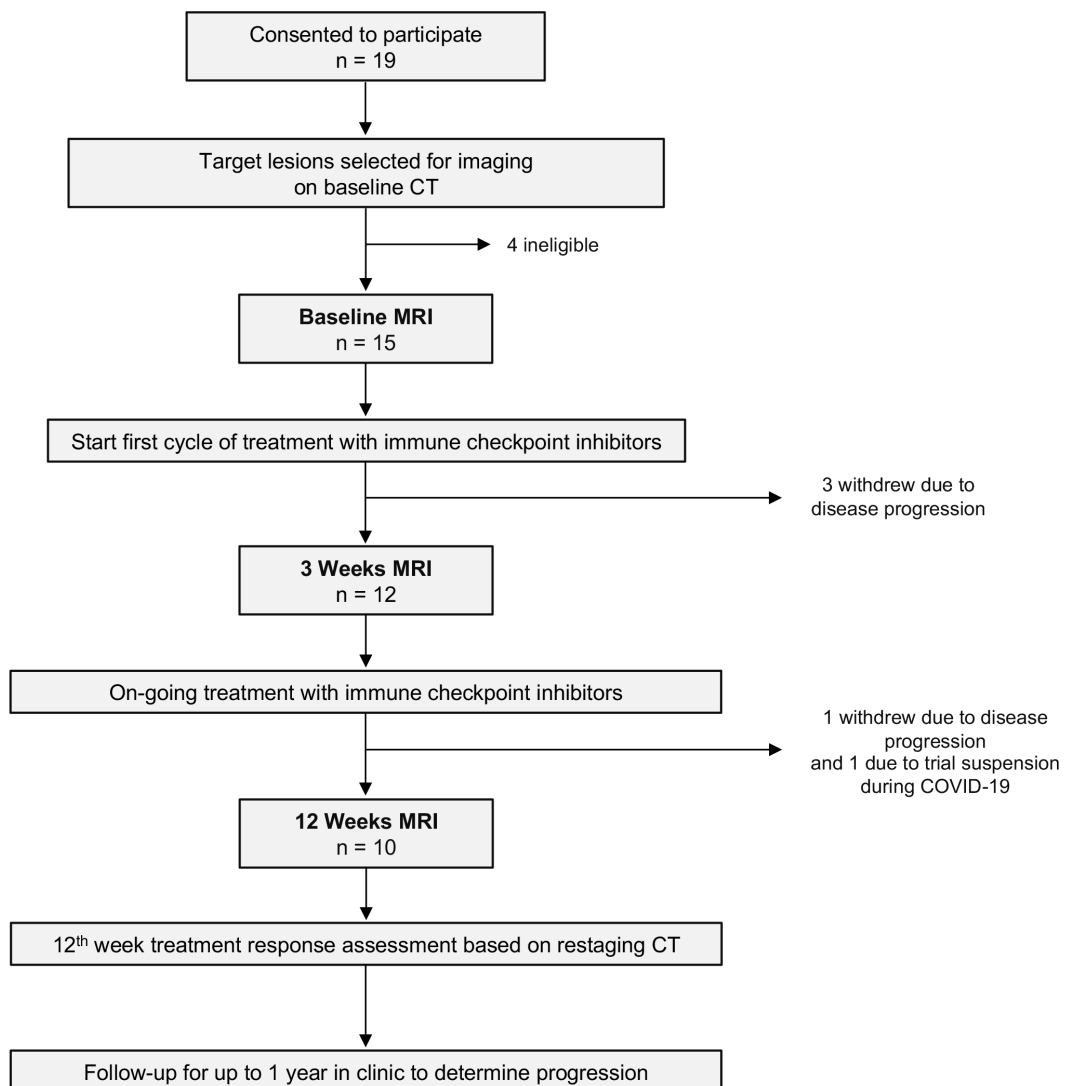
Figure 1 An mpMRI approach for longitudinal tracking of biological changes within tumors in response to immune checkpoint blockade. (A) Schematic diagram of the mpMRI approaches used in this study for monitoring tumor response to immune checkpoint blockade. K^{trans} measurements on dynamic contrast-enhanced MRI were used to quantify vascular permeability, while v_e and v_p reported on the volume of the extravascular–extracellular and vascular spaces, respectively. Diffusional kurtosis imaging, as an advanced form of diffusion-weighted imaging, was used to probe tissue microstructure using the metrics of apparent diffusivity (D_{app}) as a measure of cellularity and apparent kurtosis (K_{app}) for tissue heterogeneity. (B) Study flow chart for the melanoma immunotherapy trial (MelResist). mpMRI, multiparametric MRI.

Table 1 Clinical characteristics of study participants

Characteristics	
No. of patients	15
Age (median age, range)	65.4 (69, 48–76)
Gender	10 males, 5 females
AJCC Stage	IV
ECOG performance status	
0	9
1	6
BRAF status	
BRAF V600 mutant	3
BRAF Wild-type	12
Serum LDH (IU/mL) at baseline	
Normal (<250)	10
Elevated (>250)	5
Neutrophils-to-lymphocyte ratio at baseline	
Normal (<5)	12
High (>5)	3
Immunotherapy, n (%)	
Pembrolizumab	6 (40.0)
Nivolumab	2 (13.3)
Combined ipilimumab and nivolumab	7 (46.7)
RECIST 1.1 CT evaluation at 12th week, n (%)	
Partial response	5 (33.3)
Stable disease	4 (26.7)
Progressive disease	6 (40.0)
RECIST 1.1 CT evaluation at 1 year, n (%)	
Complete response	3 (20.0)
Partial response	4 (26.7)
Progressive disease	8 (53.3)
Anatomical site selected for MRI	
Head and neck	2
Chest	1
Abdomen and pelvis	7
Subcutaneous	4
Limbs	1

All patients imaged were histologically confirmed as AJCC Stage IV melanoma.
AJCC, American Joint Committee on Cancer staging (seventh edition); ECOG, Eastern Cooperative Oncology Group; LDH, lactate dehydrogenase; RECIST 1.1, Response Evaluation Criteria in Solid Tumors guidelines V.1.1.

table 1. Further details on the patient demographics can be found in online supplemental table S1.

Magnetic resonance imaging
All patients underwent proton (^{1}H) MRI on a 3.0 Tesla system (Discovery MR750, GE Healthcare, Waukesha, Wisconsin, USA) using a 32-channel phased-array coil with respiratory gating or multiple breath-holds used to reduce motion artifacts during image acquisition for lesions in the abdomen. The mpMRI protocol included multi-planar T_2-weighted single-shot fast spin-echo anatomical imaging, DKI of tumor cellularity and heterogeneity, and DCE-MRI of tumor perfusion or vascular permeability. Imaging was conducted at three timepoints: within 1 week prior to starting treatment with immune checkpoint inhibitors (baseline MRI); 3 weeks after the first infusion (3-week MRI) and 12 weeks after the start of treatment (12-week MRI) coinciding approximately with the first standard-of-care restaging CT response assessment at 12 weeks. Further details on the imaging acquisition, image processing and analysis can be found in the online supplemental material and table S2.

Classification of target melanoma metastases and measurement of response
Conventional objective response of the target metastases was determined by measuring the best treatment outcome at the 12-week restaging CT and reassessed at 1 year if the patient survived. Response was evaluated by standard Response Evaluation Criteria in Solid Tumors (RECIST) V.1.1 guidelines at 12 weeks and 1 year.[29]

In addition, tumor measurements were assessed using MRI during the first 12 weeks. Metastases with at least a 30% decrease in volume on the 12-week MRI were classified as responding, metastases with at least a 20% increase in volume were identified as true progression, while metastases with at least a 20% increase in volume at the 3-week MRI, but which subsequently decreased in >30% on the 12-week scan, were classified as pseudoprogression.

Statistical analysis
Statistical analysis was performed in GraphPad Prism software V.8 (La Jolla, California, USA). All values were expressed as median and IQR to account for sample size differences between groups. Normality was assessed using the Shapiro-Wilk test. Changes in individual lesion mpMRI biomarkers over the treatment timepoints were evaluated using either paired t-test for normally distributed data or Wilcoxon matched-pair signed-rank test for data with non-parametric distribution. Differences between the subgroups of responding, pseudoprogressive, and true progressive lesions were evaluated using one-way analysis of variance for normally distributed data, or the Kruskal-Wallis test with Dunn's multiple comparison for non-parametric testing. Spearman's correlation analysis was used for evaluating any relationship between the mpMRI biomarkers across treatment timepoints. A value of p<0.05 was considered as statistically significant.

RESULTS
Clinical characteristics
Fifteen treatment-naïve patients (10 males, 5 females; median age 65 years) were imaged with mpMRI over the first 12 weeks of immunotherapy. Ten patients completed MRI at all three imaging timepoints (baseline, 3-week and 12-week MRIs); 5 patients were scanned at baseline and/or 3 weeks before withdrawal from the trial due to clinical reasons such as early disease progression or clinical deterioration incompatible with continuing on the study. An

additional four patients were enrolled on the study but were deemed as ineligible for the prospective trial due to insufficient time for scheduling of imaging scans before the start of treatment (within a week) or target lesions that were too small (less than 1 cm in largest diameter) for multiple timepoint imaging and follow-up treatment response assessment. 53% of the patients received PD-1 monotherapy, while 47% of the patients were treated with combined CTLA-4 and PD-1 therapy.

Differential response to immune checkpoint blockade

Based on RECIST V.1.1 assessment at the 12-week restaging CT, five patients demonstrated partial response to immune checkpoint inhibitors, four had stable disease, and six showed disease progression. The patients with stable disease demonstrated differential response between the individual metastases. Two out of these four patients subsequently progressed at the 1-year restaging CT, and the remaining two patients demonstrated continued response to treatment (table 1). Consequently, at the 1-year timepoint, three patients showed complete response, four demonstrated partial response, one was alive with progressive disease, and the remaining seven had died from progressive disease. Further details on patient demographics can be found in online supplemental figure 1.

The mpMRI images for a total number of 27 enhancing target melanoma metastases that were first identified as more than 1 cm in diameter on staging CT were analyzed. In this study, a total of 13 responding, 4 pseudoprogressive, and 10 true progressive metastases were identified by MRI. Tumors were categorized into three subgroups (responding, pseudoprogression, and true progression) were based on comparing the 3-week MRI with the 12-week MRI, confirmed with restaging CT at 12 weeks and follow-up on the clinical outcome for up to 1 year. There were no lesions that showed a 30% decrease in volume at the 3-week MRI, which subsequently increased in volume at the 12-week MRI or on the restaging CT.

T_2-MRI volumetric analysis showed differential inter-patient and intermetastatic response to immune checkpoint blockade. Within the cohort of patients in our study, intermetastatic differences in the individual tumor growth kinetics were particularly evident in patients undergoing anti-PD-1 monotherapy, as compared with patients receiving combined CTLA-4 and PD-1 treatment, where response was almost immediate at the 3-week MRI (figure 2A), which may represent the fact that monotherapy takes longer to mount antitumor effects compared with combination therapy. Interestingly, increasing T_2 hyperintensity or inflammatory changes were detected within all four enlarged pseudoprogressive tumors at 3 weeks, which resolved at 12 weeks with a corresponding reduction in tumor volume (figure 2B and figure 3).

Tumor cell death and changes in heterogeneity in response to treatment

Figure 4 and online supplemental figure S1 show the changes in tumor cellularity and heterogeneity measured on DKI. No significant difference in the average D_{app} for each patient, as a measure of tumor cell density, was detected between the responding and non-responding patients at baseline (figure 4A); median D_{app} of 1.44 for responding patients versus 1.33 for non-responding patients, p=0.62). There was a significant increase in the average D_{app} of imaged target metastases for each patient representing reduced tumor cellularity (p<0.05) in the responding patients at 3 weeks (median D_{app} 1.65; IQR 1.59–1.77) compared with baseline (1.44; IQR 1.26–1.63), with a further significant increase at 12 weeks (2.01; IQR 1.60–2.22). In contrast, there was no significant change in D_{app} in the tumors of non-responders over the 12 weeks of treatment (figure 4B).

Further analysis based on classification of individual metastases from all patients into the three subgroups of 'responding', 'pseudoprogression' and 'true progression', showed a significantly lower D_{app}, reflecting higher tumor cell density at baseline in the pseudoprogressive lesions (median 1.17; IQR 1.02–1.20), as compared with the responding (median 1.48; IQR 1.44–1.68; p<0.001) and true progressive lesions (median 1.44; IQR 1.15–1.82; p<0.05). Individual tumors responded differently to treatment: most of the responding and pseudoprogressive lesions exhibited a significant percentage increase in D_{app} at the 3-week MRI relative to baseline, indicating lower cellularity in most responding lesions (median increase in D_{app} by 8.9%; IQR 2.3%–27.6%; p<0.05) and pseudoprogressive lesions (median increase by 48.0%; IQR 45.2%–63.1%; p<0.05). A further increase in D_{app} was detected within the tumor microenvironment in most of the metastases responding at 12 weeks (31.7%; IQR 1.9%–45.5%; p<0.05). However, one lesion demonstrated higher cellularity (increase in D_{app}) despite a reduction of tumor volume over 12 weeks of treatment; interestingly, this lesion subsequently increased in size at the sixth month restaging CT and was verified to be a pseudoprogressive lesion over a longer timeframe. Higher cellularity was also detected on average in the pseudoprogressive lesions at 12 weeks compared with the responding lesions, despite a reduction in tumor volume, which may reflect a later phase of immune infiltration and tumor cell killing in these metastases (figures 4 and 5). This patient demonstrated complete response on RECIST V.1.1 evaluation at the 1-year follow-up CT scan. Overall, the D_{app} values measured from the experimental DKI images correlated to the apparent diffusion coefficient (ADC) values obtained on clinical DWI for all imaged patients (online supplemental figure S2).

No significant difference in microscopic tumor heterogeneity at baseline (p=0.27) was detected in the tumors of the responders (median K_{app} 0.61; IQR 0.51–0.71), compared with non-responding patients (median 0.71; IQR 0.53–0.86), as detected by the average apparent
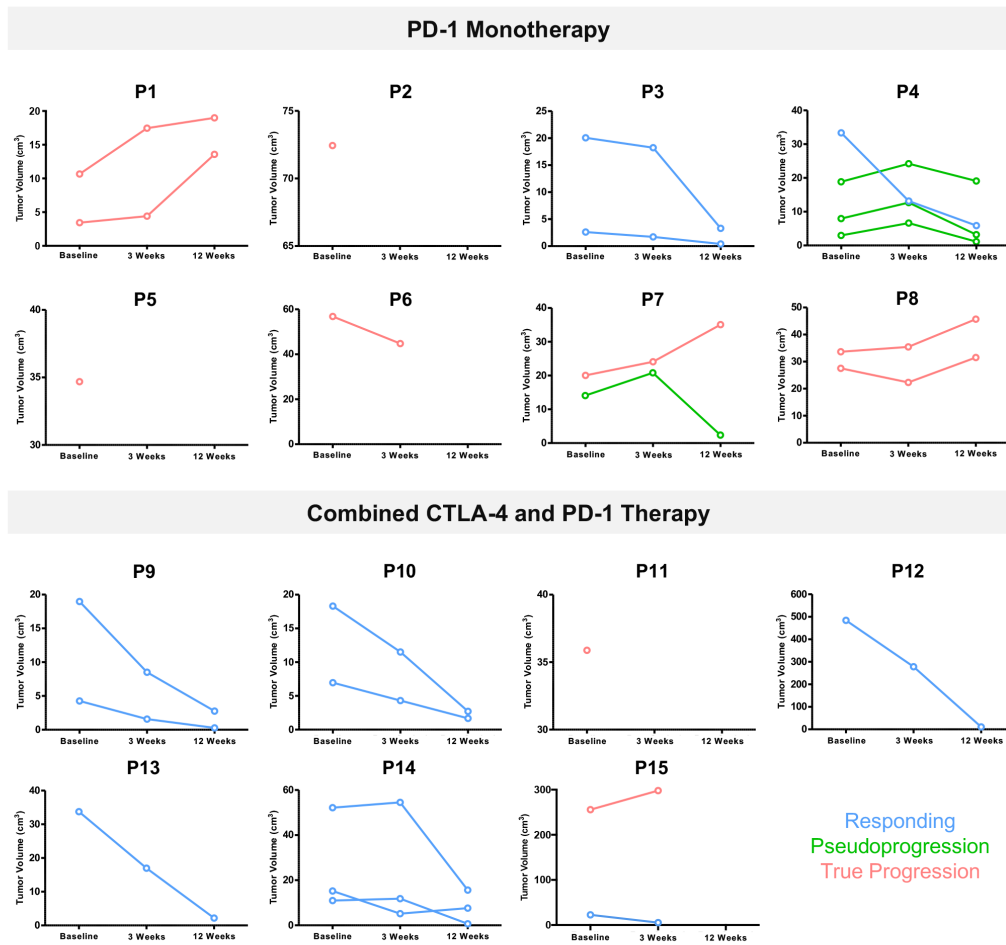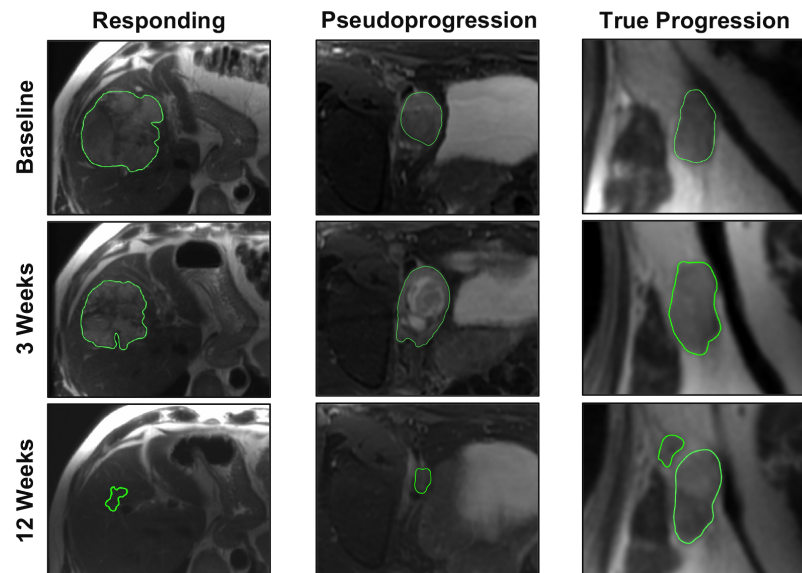
Figure 2 Interpatient and intermetastatic heterogeneity in response to immune checkpoint blockade. (A) Differential tumor growth kinetics in patients receiving PD-1 monotherapy compared with combined CTLA-4 and PD-1 treatment. Individual tumor volumes were measured on T_2-weighted MRI. Categorization of tumors into three subgroups (responding, pseudoprogression, and true progression) were based on comparing the 3-week MRI with the 12-week MRI, confirmed with restaging CT at 12 weeks and follow-up on the clinical outcome for up to 1 year. (B) Representative T_2-weighted images from three patients with the classic features of responding, pseudoprogressive, and true progressive lesions. Note the T2 hyperintensity in keeping with inflammation in the pseudoprogressive lesion at 3 weeks. CTLA-4, cytotoxic T-lymphocyte antigen-4; PD-1, programmed cell death receptor-1.
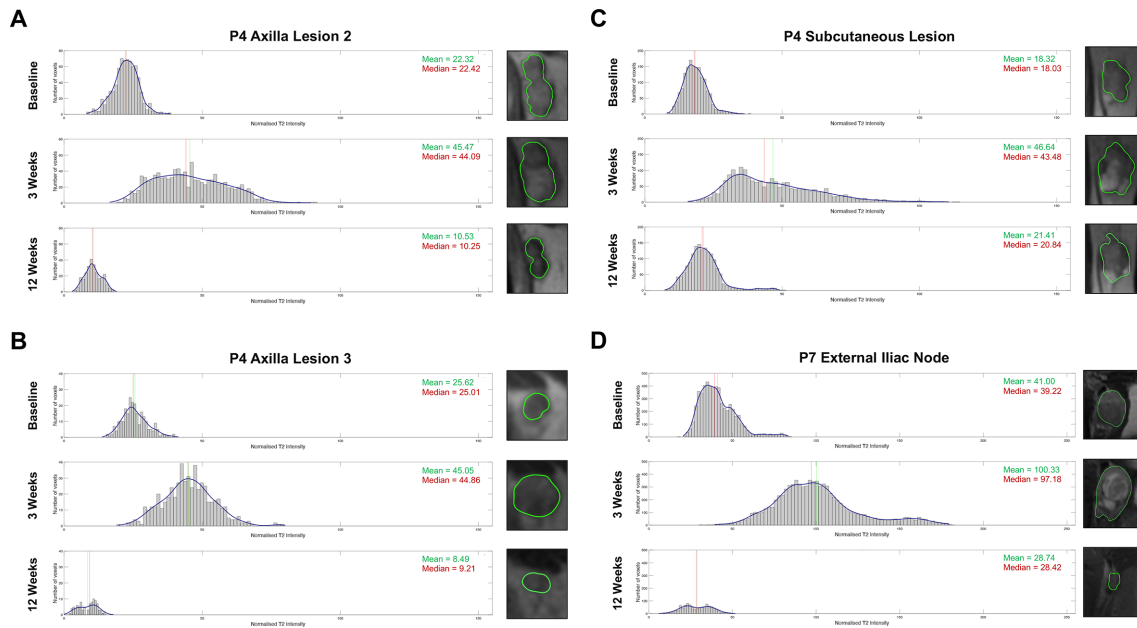
Figure 3 Histogram analysis of the T_2 intensity values of all four pseudoprogressive lesions.[8] These included: the (A) axilla lesion 2, (B) axilla lesion 3, (C) subcutaneous lesion of patient 4, and the (D) external iliac node of patient 7.

kurtosis (K_{app}) values from all target lesions for each patient obtained concurrently on DKI (online supplemental figure S1). A significant reduction in K_{app} (p<0.05) was detected in the tumors of responding patients at 3 weeks (median 0.59; IQR 0.51–0.65) compared with baseline (median 0.61; IQR 0.51–0.71). Further analysis of the individual lesions showed a trend towards a higher level of tumor heterogeneity, as measured by K_{app}, in the pseudoprogressive lesions throughout the first 12 weeks of treatment (baseline: 0.84; 3 weeks: 0.64; 12 weeks: 0.76) compared with the responding lesions (baseline: 0.59; 3 weeks: 0.54; 12 weeks: 0.56); although this did not reach statistical significance, it may reflect underlying immune cell infiltration or cell death over the course of treatment. As with the results for D_{app}, no significant change in K_{app} was detected in the progressing metastases during the first 12 weeks of treatment.

Tumor vascular remodeling following cell death

Figure 6 and online supplemental figure S3 show the changes in tumor vascularity and perfusion during 12 weeks of treatment, as measured by DCE-MRI and contrast kinetic modeling using the extended Tofts model. The average tumor vascular transfer constant (K^{trans}) at baseline was higher in the target lesions of the responding patients (median K^{trans} 0.56; IQR 0.23–1.37) compared with the non-responders (0.15; IQR 0.11–0.44; p<0.05). Similarly, the average fractional extravascular–extracellular volume (v_e) at baseline of the target lesions of the responding patients were higher (median v_e 0.49; IQR 0.31–0.77) compared with the non-responders (0.19; IQR 0.15–0.32; p<0.05). A significant reduction in these tumor vascularity metrics (K^{trans}, v_e, and v_p) was only detected at 12 weeks compared with baseline (0.11; IQR 0.05–0.45; p<0.05) but not at 3 weeks. A gradual increase in tumor

vascular metrics was detected in the tumors of non-responding patients over the course of treatment, but this was not statistically significant, which may reflect the small numbers, particularly at the 12-week MRI. Further analysis on the individual lesions showed no significant difference in the vascular transfer constant K^{trans}, fractional volume of the extravascular–extracellular space v_e, or fractional plasma volume v_p, between the three subgroups of lesions before the start of treatment. A significant decrease in K^{trans} relative to baseline was detected in most responding lesions at 12 weeks (median −66.19%; IQR −92.00 to −46.49%; p<0.01) but not at the 3-week MRI (−29.73%; IQR −40.51 to 14.01%; p=0.23). Similarly, v_e and v_p were also lower in the responding lesions at 12 weeks (p=0.07 and p<0.01, respectively). A trend towards lower K^{trans} was also detected in most pseudoprogressive lesions at 3 weeks (median 0.47; IQR 0.18–0.60) and 12 weeks (0.15; IQR 0.11–0.32), compared with baseline (0.52; IQR 0.19–0.82), but this was not statistically significant given the small number of pseudoprogressive lesions within the patient cohort.

Early treatment timepoint changes in tumor cellularity is independent of tumor volume

Spearman's correlation analysis of the mpMRI biomarkers over the first 12 weeks of treatment in this cohort showed no significant correlation between tumor volume and D_{app} (online supplemental figure S4). This implies that the early detection of changes in tumor cellularity from immune cytotoxic killing of tumor cells at the 3-week MRI was independent of changes in tumor volume. However, a positive correlation was found between tumor volume and all metrics of tumor vascularity and perfusion at 12 weeks (K^{trans}, v_e, and v_p), suggesting that vascular remodeling
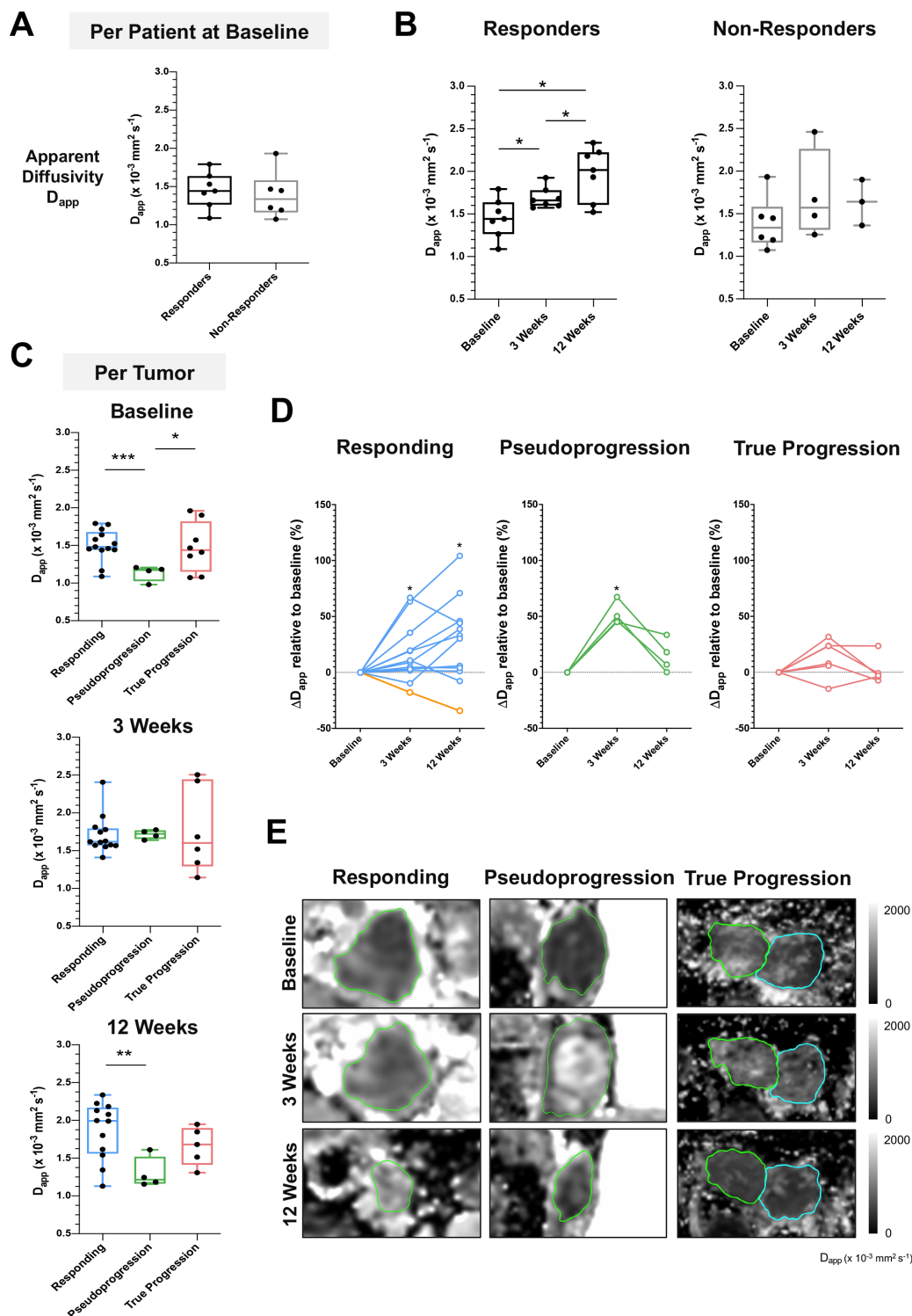
Figure 4 Early detection of tumor cell death using DKI. (A) Comparison of apparent diffusivity (D_{app}) as a measure of tumor cell density between responders and non-responders at baseline before the start of treatment. (B) Changes in average tumor D_{app} on a per patient basis over the course of treatment, divided according to overall response. (C) Response of individual lesions classified into three subgroups (responding, pseudoprogression, and true progression) showing the differences in tumor cellularity at baseline. (D) Percentage change in D_{app} relative to baseline in individual lesions from the three subgroups. (E) Representative D_{app} images from three lesions categorized as responding, pseudoprogression, and true progression, respectively, based on the 1-year restaging CT. Data are presented as median and IQR. Normality was assessed using the Shapiro-Wilk test. Mann-Whitney test was performed to assess differences between two independent lesion subgroups; Kruskal-Wallis test with post hoc Dunn's multiple comparison analysis was performed to test for differences between three independent lesion subgroups; *p<0.05; ***p<0.001. Yellow line in figure part D indicates the percentage change in D_{app} for patient 4. Analysis of apparent kurtosis as a measure of tumor heterogeneity, detected concurrently using DKI, is found in online supplemental figure S1. DKI, diffusion kurtosis imaging.
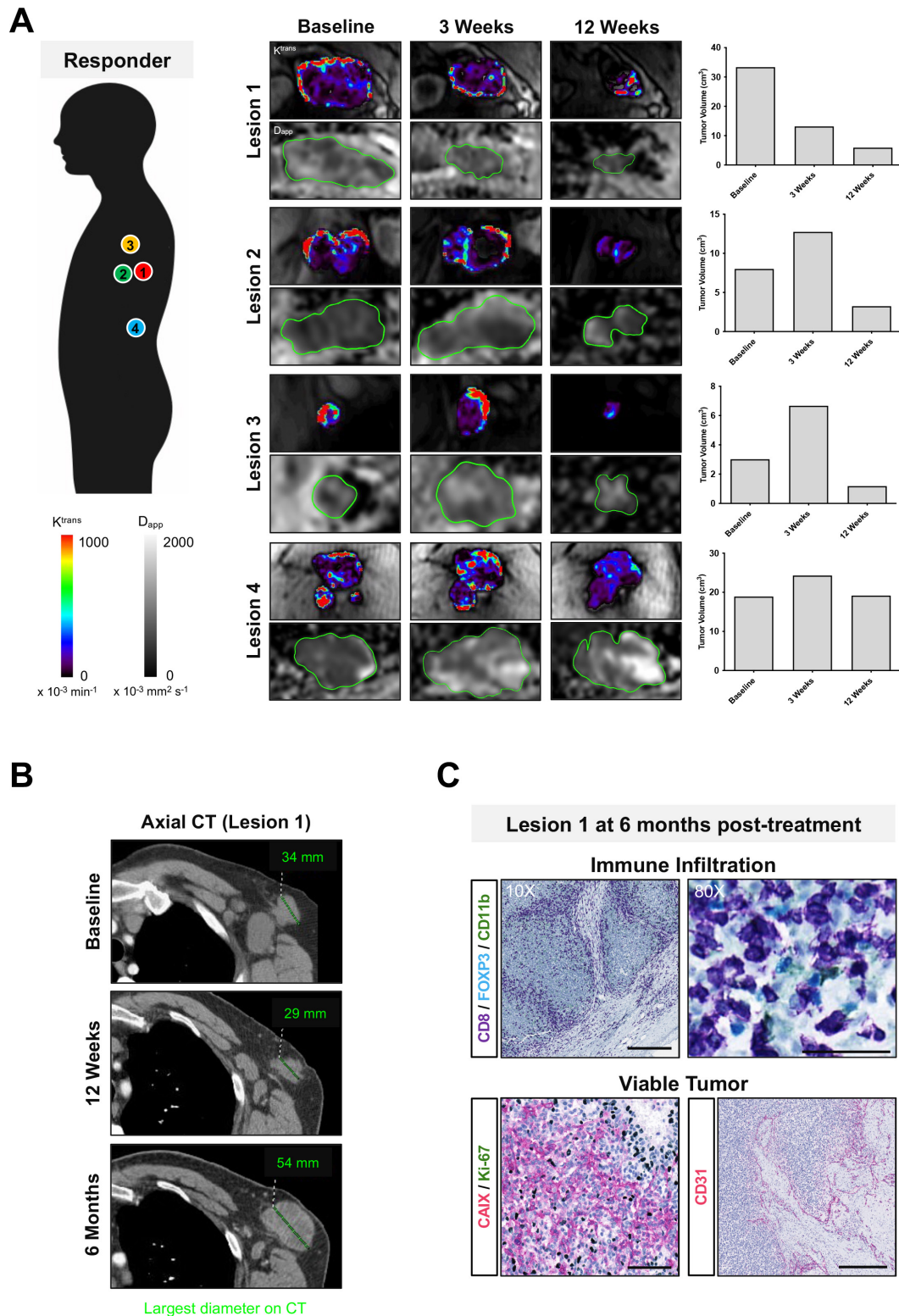
Figure 5 Dynamic changes in intertumoral response to immune checkpoint blockade within a single patient. (A) Multiple metastases in a patient on treatment with nivolumab (PD-1 monotherapy). Intertumoral differences in treatment response, vascular permeability, and cellularity were measured in four target lesions on MRI during the first 12 weeks of treatment. Increased cellularity was detected in the responding tumor (lesion 1) despite a reduction in tumor volume and lower vascularity at 12 weeks. The responding lesion subsequently progressed at 6 months on treatment and was surgically resected. (B) Axial CT of lesion 1 at baseline, 12 weeks, and 6 months; largest tumor diameter shown in mm. (C) Immunohistochemistry of lesion 1 showed remarkable infiltration of immune cells (CD8) in viable tumor tissues that were highly hypoxic (CAIX), proliferative (Ki67), and vascular (CD31). Scale bars for CD8 immunostained images represent 100 μm (10× magnification) and 50 μm (80× magnification); 100 μm in CAIX/Ki67 dual staining (20× magnification) and CD31 (10× magnification). PD-1, programmed cell death receptor-1.
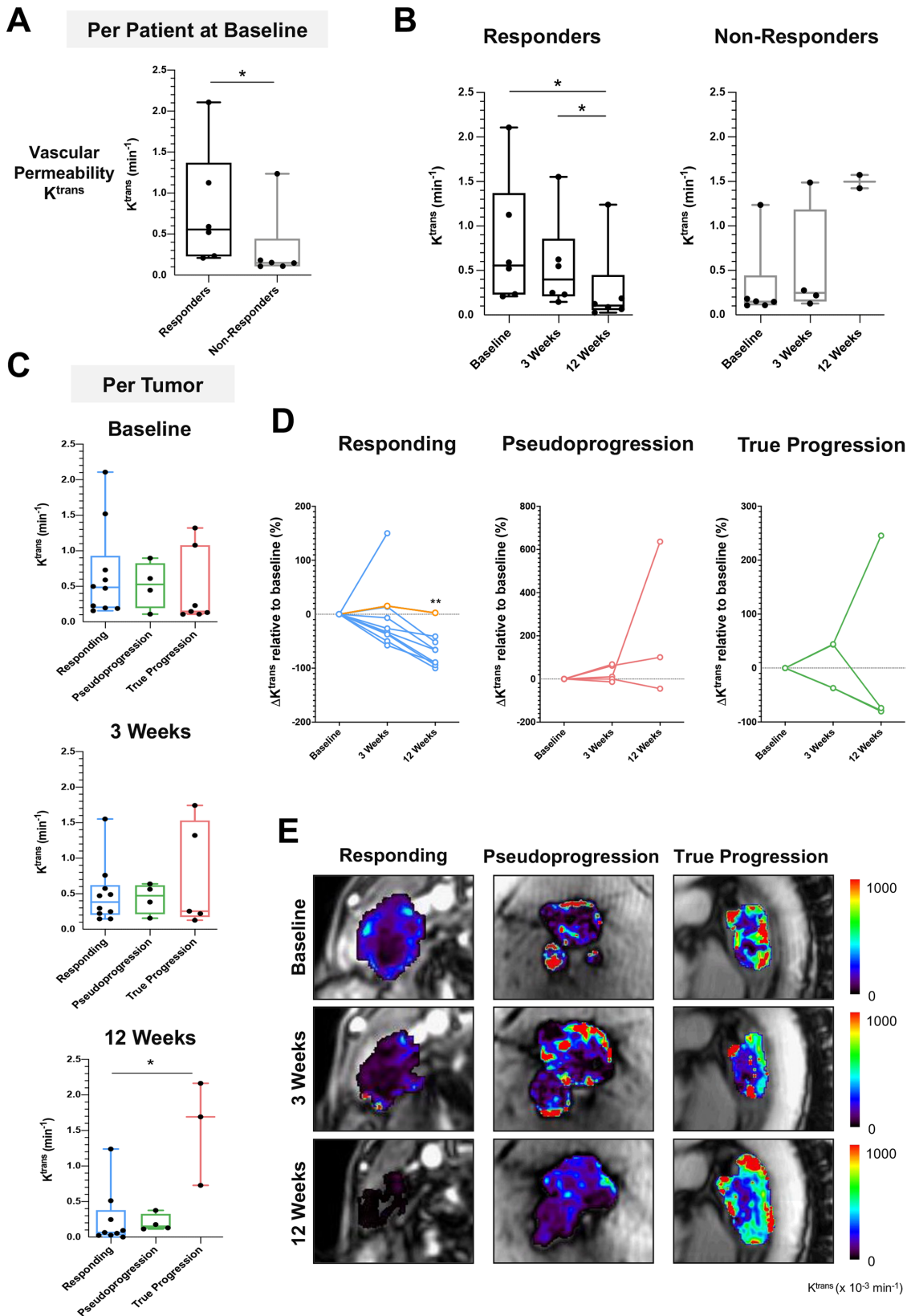
Figure 6 Tumor vasculature remodeling following immune cytotoxic killing and tumor cell death. (A) Comparison of vascular permeability K^{trans} between responders and non-responders at baseline before the start of treatment. (B) Changes in tumor K^{trans} over the course of treatment. (C) Comparison of tumor vascular permeability at baseline between individual lesions from the three subgroups: responding, pseudoprogression, and true progression. (D) Percentage change in K^{trans} relative to baseline in individual lesions from the three subgroups. (E) Representative K^{trans} images from the three subgroups lesions. $*P<0.05$; $**p<0.01$. Yellow line in figure part D indicates the percentage change in K^{trans} for patient 4. Analysis for other DCE-MRI parametric measurements is found in online supplemental figure S3. DCE-MRI, dynamic contrast-enhanced MRI.

may be related to tumor size changes following immune checkpoint blockade.

DISCUSSION

As immune checkpoint inhibitors become more widely used in routine clinical practice, there is an unmet need for more effective tools to measure successful response to these agents. This is increasingly important as more patients with cancer are being offered long term immunotherapy, which is costly to healthcare systems and comes with a significant risk of side effects. Tumor heterogeneity is one of the major challenges for effective cancer treatment and manifest as morphological, functional, cellular, metabolic, and molecular diversity.[30][31] Clinical tools to image this multilayered tumor heterogeneity and how it changes with immunotherapy could have a role in differentiating tumor resistance from successful response early in the treatment pathway.[32]

In this study, longitudinal tracking of microstructural and functional changes in metastatic melanoma during the first 12 weeks of treatment was performed using mpMRI. Heterogeneity in response to immune checkpoint blockade was observed in these treatment-naïve tumors. This heterogeneity may be due to interpatient and intermetastatic differences in tumor immunogenicity, as some patients may have more delayed response, multiple waves of immune activation or ongoing immune evasion and clonal expansion during continuous treatment, as exemplified by patient 4. These changes in the tumor microenvironment may not be identified by standard CT or MRI, as the change in tumor size alone are often insufficient to determine treatment benefit at the early stages of immunotherapy. Therefore, a clinically applicable tool to evaluate immunotherapy is required to guide clinical decision making.[33]

Treatment response to immune checkpoint blockade was captured longitudinally on mpMRI in this study using three approaches to assess the tumor microenvironment: T_2-weighted MRI of tissue structure, DKI of cellular density and its microscopic heterogeneity, and DCE-MRI of the tumor vasculature. An interesting and unexpected observation was an increase in median T_2-weighted signal intensity following 3 weeks of immunotherapy (one infusion of immunotherapy) in the pseudoprogressive metastases, compared with metastases that responded or were shown to progress at later timepoints. This is likely to be due to tumor enlargement from significant immune cell infiltration and inflammation, rather than tumor proliferation. T_2-weighted MRI represents a very simple routine clinical tool that may be able to discriminate pseudoprogression from true progression if this initial observation could be confirmed in larger studies. Quantitative analysis of these signal intensity changes, for example, using T_2 mapping, may be useful in future trials for more detailed characterization of these microstructural changes.[34]

Changes in cell density were measured using D_{app} on DKI to detect either cytotoxic T-cell killing or increased cell density from immune infiltration or tumor proliferation. Cell loss measured as an increase in the median D_{app} was detected in both responding and pseudoprogressive lesions as early as 3 weeks after the start of treatment compared with baseline. Further reductions in cell density within the responding lesions were detected at the 12-week MRI. An increase in ADC measured on DWI (equivalent to the D_{app} measured here) has also been reported in previously treated ocular melanoma responding to immunostimulatory adenoviral CD40L gene therapy: ≥1 fold change in ADC at week 5 following treatment was a better predictor of objective survival than metabolic changes on ^{18}F-FDG PET and tumor size changes on MRI.[35] Interestingly, in our study, an increase in cell density (or lower D_{app}) was detected in the pseudoprogressive lesions at 12 weeks compared with the responding lesions, despite reduced tumor volumes measured on the 12-week MRI and standard restaging CT. No significant correlation between D_{app} and tumor volume was detected across the imaging timepoints, which implies that the estimation of cell density based on water diffusion within the tumor microenvironment is independent of tumor volume and is therefore an important additional metric to measure. A higher degree of tumor heterogeneity, as assessed by an increase in K_{app}, was detected in the pseudoprogressive lesions throughout the MRI imaging timepoints, compared with the responding lesions. This supports the hypothesis that there is underlying cellular alteration with different phases of immune activation and proliferation in the pseudoprogressive lesions over the course of treatment. Although there was a higher K_{app} in the true progressive lesions at all imaging timepoints compared with the responding lesions, the feasibility of using DKI alone to differentiate true progression from pseudoprogression could not be established as the number of non-responders with complete MRI scans are limited in the metastatic disease setting due to early disease progression and withdrawal from the trial. Nevertheless, greater tumor heterogeneity at baseline (entropy, dissimilarity, and contrast texture features) measured on CT radiomics has been previously reported in non-responders to PD-1 monotherapy.[36]

The tumor vasculature plays a significant role in regulating tumor homeostasis, metastasis, and immune trafficking.[37] The vascular networks in malignant tumors are typically disorganized with immature, tortuous, and leaky blood vessels that are hyperpermeable to intravascular contrast agents. DCE-MRI showed a gradual decrease in: the tumor vascular permeability K^{trans}; the extravascular–extracellular space v_e; and the plasma volume fraction v_p within the responding lesions. This was more prominent at the 12-week MRI when a reduction in tumor burden was detected, suggesting that tumor vasculature remodeling and shutdown may have occurred following cell death caused by cytotoxic T cell killing. This contrasts with the effects of antiangiogenic treatments in human melanoma xenografts whereby the treatments are more directed towards the vascular network and are generally

not cytotoxic. Tumor vasculature remodeling as represented by a lower K^{trans}, often precedes cell death and reduction in tumor burden, with no significant change in cell density measurements such as v_e or ADC.[38] Despite the small number of pseudoprogressive lesions available for analysis in our study, lower K^{trans}, v_e and v_p, with a corresponding reduction in tumor volume because of cell death, was detectable in most pseudoprogressive lesions at 12 weeks. The pseudoprogressive lesions in general demonstrated lower vascular permeability and perfusion compared with the true progressive lesions at 12 weeks. Our findings are in concordance with a previous study assessing DCE-MRI melanoma brain metastases study in which lower v_p was detected in previously irradiated pseudoprogressive lesions compared with true progressive lesions after three cycles of ipilimumab.[24] This suggested that DCE-MRI may have utility in distinguishing true progressive lesions from treatment-responsive lesions but at a later timepoint compared with diffusion measurements. Interestingly, higher K^{trans} and v_e were detected at baseline in all imaged tumors of most patients who were responders to immune checkpoint inhibitors compared with the non-responders. One explanation could be that the differences in tumor vasculature between tumors may play a role in determining immune trafficking and subsequent immune eradication of tumor cells.[37] Ideally, this could be explored by tissue sampling of multiple lesions both before and during therapy, but this is not practical in the metastatic disease setting clinically, and further preclinical research is required.

As part of this prospective study, we have demonstrated marked intralesional, intermetastatic, and interpatient heterogeneity in melanoma over the first 12 weeks of immunotherapy. After only 3 weeks of treatment or one infusion of immunotherapy, a decrease in cellularity, as measured on DKI, could distinguish responding patients from non-responders, as well as individual responding and pseudoprogressing tumors from true progressing ones. An interesting finding was an increase in normalized T_2-weighted signal and its distribution in the pseudoprogressing lesions compared with the progressing lesions after 3 weeks treatment. Therefore, combining conventional T_2-weighted and DKI at 3 weeks after starting immunotherapy could be used to identify pseudoprogression during the early stages of treatment. Although there was higher tumor vascular permeability and perfusion at baseline in the responding patients on DCE-MRI compared with non-responders, changes in K^{trans} could not be used to distinguish responding and pseudoprogressing lesions until after 12 weeks of treatment showing that measurable vascular changes occur later than changes in cellularity.

Our study presented several strengths and limitations. This is the first prospective MRI study to serially track cellular and functional changes in melanoma metastases during immune checkpoint blockade. As all melanoma metastases analyzed in this study were previously untreated and unresectable tumors, the treatment timepoint changes measured on mpMRI were directly related to immunotherapeutic effects on individual lesions. Partial volume effects on image measurements were minimal as several patients in our trial presented large metastases at baseline. A stringent criterion for imaging and analysis was maintained to include only patients with measurable disease so that the biological changes were trackable over 12 weeks of immunotherapy. Nevertheless, our study is limited by the small sample size, which restricts the scope for wider interpretation of the results and evaluation of the imaging biomarkers for their predictive values. Future multicenter trials are required to test and validate these imaging biomarkers in a larger patient cohort, with the aim of integrating these imaging methods into immunotherapy trials and routine clinical management. Our study is further limited by the lack of radiological–pathological correlation, as relatively few metastases are readily accessible to biopsy. This difficulty in obtaining tumor tissues from metastatic sites further highlights the strengths of non-invasive imaging as a surrogate for pathology as changes in tumor growth kinetics, cell density, heterogeneity, and vascularity within individual tumors could be longitudinally tracked over the course of treatment.

Although no CT was available at the 3-week MRI timepoint for direct comparison, the lesional volume on MRI at this early timepoint represents a surrogate for the CT size measurements. Using size criteria alone, conventional CT is unlikely to provide additional information over MRI. The latter not only provides enhanced soft tissue contrast, but importantly can probe quantitative measures of tissue function that are not possible with CT, thus providing significant biological information as we have demonstrated here. Although CT can be used to probe tumor perfusion as part of dynamic contrast-enhanced CT, this is usually at lower temporal resolution and with a significant radiation burden given the multiple acquisition timepoints. More generally, the radiation dose from CT decreases its suitability for multiple timepoint imaging, especially in patients who are particularly at risk of radiation effects. The emerging field of radiomics to study tissue heterogeneity would also be interesting to evaluate on CT at this early 3-week timepoint, but both radiomics and CT perfusion are currently research tools and require validation within future prospective trials.

In conclusion, mpMRI has shown potential for early assessment of response to immunotherapy in metastatic melanoma patients. Early changes in tumor cellularity measured on DKI following 3 weeks after starting treatment could be used to detect responding and pseudoprogressive melanoma metastases before a change in tumor volume and vascular permeability. This work could have important implications for monitoring treatment of metastatic melanoma and the increasing number of solid cancers treated with immunotherapy.

Author affiliations
[1]Department of Radiology, University of Cambridge, Cambridge, UK
[2]Cancer Research UK Cambridge Centre, Cambridge, UK

[3]Department of Radiology, Addenbrooke's Hospital, Cambridge, UK
[4]Department of Oncology, Cambridge University Hospitals NHS Foundation Trust, Addenbrooke's Hospital, Cambridge, UK
[5]Clinical Pharmacology & Safety Sciences, AstraZeneca PLC, Cambridge, Cambridgeshire, UK
[6]Department of Nuclear Medicine, Addenbrooke's Hospital, Cambridge, UK
[7]Cancer Research UK Cambridge Research Institute, Cambridge, UK

Twitter Doreen Lau @DoreenLau4 and Ferdia A Gallagher @FerdiaGallagher

Contributors Conceptualization of study: DL, FAG, PGC, MAM, MJG, and KMB. Data curation and formal analysis: DL, FAG, PGC, MAM, ANP, ABG, and FS. Investigation: DL, FAG, PGC, MAM, and ANP. Methodology: DL, MAM, ANP, ABG, IP, BC, FR, JDK, MJG, MS, and LB. Resources: AF, DM, CB, AL, MS, LB, J-ML, and LA. Writing – original draft: DL, FAG, and PGC. Writing – review and editing: DL, MAM, ANP, ABG, FAG, and PGC.

Competing interests No conflict of interest to declare with respect to the content of this work. AL, MS, LB, and J-ML are employees of AstraZeneca UK.

Patient consent for publication Obtained.

Ethics approval MelResist is a prospective study approved by the local institutional review board and research ethics committee (11/NE/0312) and managed within the Cambridge Clinical Trials Unit, Cambridge University Hospitals National Health Service Foundation Trust, Cambridge, UK. Written informed consent was obtained from all patients before enrolment.

Provenance and peer review Not commissioned; externally peer reviewed.

Data availability statement Data are available on reasonable request. Data may be obtained from a third party and are not publicly available. All data relevant to the study are included in the article or uploaded as supplementary information. Please contact the corresponding author Doreen Lau (la399@cam.ac.uk).

Supplemental material This content has been supplied by the author(s). It has not been vetted by BMJ Publishing Group Limited (BMJ) and may not have been peer-reviewed. Any opinions or recommendations discussed are solely those of the author(s) and are not endorsed by BMJ. BMJ disclaims all liability and responsibility arising from any reliance placed on the content. Where the content includes any translated material, BMJ does not warrant the accuracy and reliability of the translations (including but not limited to local regulations, clinical guidelines, terminology, drug names and drug dosages), and is not responsible for any error and/or omissions arising from translation and adaptation or otherwise.

ORCID iDs
Doreen Lau http://orcid.org/0000-0002-7623-2401
Mary A McLean http://orcid.org/0000-0002-3752-0179
Andrew N Priest http://orcid.org/0000-0002-9771-4290
Andrew B Gill http://orcid.org/0000-0002-9287-9563
Jean-Martin Lapointe http://orcid.org/0000-0003-0141-4603
Pippa G Corrie http://orcid.org/0000-0003-4875-7021
Ferdia A Gallagher http://orcid.org/0000-0003-4784-5230

REFERENCES

1 Ribas A, Wolchok JD. Cancer immunotherapy using checkpoint blockade. *Science* 2018;359:1350–5.
2 Danson S, Hook J, Marshall H, *et al*. Are we over-treating with checkpoint inhibitors? *Br J Cancer* 2019;121:629–30.
3 Schachter J, Ribas A, Long GV, *et al*. Pembrolizumab versus ipilimumab for advanced melanoma: final overall survival results of a multicentre, randomised, open-label phase 3 study (KEYNOTE-006). *Lancet* 2017;390:1853–62.
4 Larkin J, Chiarion-Sileni V, Gonzalez R, *et al*. Five-year survival with combined nivolumab and ipilimumab in advanced melanoma. *N Engl J Med* 2019;381:1535–46.
5 Larkin J, Chiarion-Sileni V, Gonzalez R, *et al*. Combined nivolumab and ipilimumab or monotherapy in untreated melanoma. *N Engl J Med* 2015;373:23–34.
6 Welsh SJ, Corrie PG. Biomarkers predicting for response and relapse with melanoma systemic therapy. *Acta Derm Venereol* 2020;100:adv00142.
7 Bedard PL, Hansen AR, Ratain MJ, *et al*. Tumour heterogeneity in the clinic. *Nature* 2013;501:355–64.
8 Gill AB, Rundo L, Wan JCM, *et al*. Correlating radiomic features of heterogeneity on CT with circulating tumor DNA in metastatic melanoma. *Cancers* 2020;12:3493.
9 Nishino M, Giobbie-Hurder A, Manos MP, *et al*. Immune-related tumor response dynamics in melanoma patients treated with pembrolizumab: identifying markers for clinical outcome and treatment decisions. *Clin Cancer Res* 2017;23:4671–9.
10 Wolchok JD, Hoos A, O'Day S, *et al*. Guidelines for the evaluation of immune therapy activity in solid tumors: immune-related response criteria. *Clin Cancer Res* 2009;15:7412–20.
11 Tan AC, Emmett L, Lo S, *et al*. FDG-pet response and outcome from anti-PD-1 therapy in metastatic melanoma. *Ann Oncol* 2018;29:2115–20.
12 Chiou VL, Burotto M. Pseudoprogression and immune-related response in solid tumors. *J Clin Oncol* 2015;33:3541–3.
13 Pandit-Taskar N, Postow MA, Hellmann MD, *et al*. First-in-humans imaging with [89]Zr-Df-IAB22M2C anti-CD8 Minibody in patients with solid malignancies: preliminary pharmacokinetics, biodistribution, and lesion targeting. *J Nucl Med* 2020;61:512–9.
14 Bensch F, van der Veen EL, Lub-de Hooge MN, *et al*. [89]Zr-atezolizumab imaging as a non-invasive approach to assess clinical response to PD-L1 blockade in cancer. *Nat Med* 2018;24:1852–8.
15 Niemeijer AN, Leung D, Huisman MC, *et al*. Whole body PD-1 and PD-L1 positron emission tomography in patients with non-small-cell lung cancer. *Nat Commun* 2018;9:1–5.
16 Liu Z, Li Z, Qu J, *et al*. Radiomics of multiparametric MRI for pretreatment prediction of pathologic complete response to neoadjuvant chemotherapy in breast cancer: a multicenter study. *Clin Cancer Res* 2019;25:3538–47.
17 Bedair R, Priest AN, Patterson AJ, *et al*. Assessment of early treatment response to neoadjuvant chemotherapy in breast cancer using non-mono-exponential diffusion models: a feasibility study comparing the baseline and mid-treatment MRI examinations. *Eur Radiol* 2017;27:2726–36.
18 McRobbie DW, Moore EA, Graves MJ. Part II - The Specialist Stuff. In: *Mri from picture to proton*. 3rd edition. Cambridge University Press, 2017. ISBN: 9781107706958.
19 Hylton N. Dynamic contrast-enhanced magnetic resonance imaging as an imaging biomarker. *J Clin Oncol* 2006;24:3293–8.
20 Patterson DM, Zweifel M, Middleton MR, *et al*. Phase I clinical and pharmacokinetic evaluation of the vascular-disrupting agent OXi4503 in patients with advanced solid tumors. *Clin Cancer Res* 2012;18:1415–25.
21 Horsley L, Cummings J, Middleton M, *et al*. A phase 1 trial of intravenous 4-(N-(S-glutathionylacetyl)amino) phenylarsenoxide (GSAO) in patients with advanced solid tumours. *Cancer Chemother Pharmacol* 2013;72:1343–52.
22 Hu D-E, Beauregard DA, Bearchell MC, *et al*. Early detection of tumour immune-rejection using magnetic resonance imaging. *Br J Cancer* 2003;88:1135–42.
23 Riegler J, Gill H, Ogasawara A, *et al*. VCAM-1 density and tumor perfusion predict T-cell infiltration and treatment response in preclinical models. *Neoplasia* 2019;21:1036–50.
24 Umemura Y, Wang D, Peck KK, *et al*. DCE-MRI perfusion predicts pseudoprogression in metastatic melanoma treated with immunotherapy. *J Neurooncol* 2020;146:339–46.

25 Papaevangelou E, Almeida GS, Jamin Y, *et al*. Diffusion-weighted MRI for imaging cell death after cytotoxic or apoptosis-inducing therapy. *Br J Cancer* 2015;112:1471–9.

26 Barrett T, McLean M, Priest AN, *et al*. Diagnostic evaluation of magnetization transfer and diffusion kurtosis imaging for prostate cancer detection in a re-biopsy population. *Eur Radiol* 2018;28:3141–50.

27 Deen SS, Priest AN, McLean MA, *et al*. Diffusion kurtosis MRI as a predictive biomarker of response to neoadjuvant chemotherapy in high grade serous ovarian cancer. *Sci Rep* 2019;9:1–9.

28 Goodburn RJ, Barrett T, Patterson I, *et al*. Removing rician bias in diffusional kurtosis of the prostate using real-data reconstruction. *Magn Reson Med* 2020;83:2243–52.

29 Eisenhauer EA, Therasse P, Bogaerts J, *et al*. New response evaluation criteria in solid tumours: revised RECIST guideline (version 1.1). *Eur J Cancer* 2009;45:228–47.

30 Grzywa TM, Paskal W, Włodarski PK. Intratumor and intertumor heterogeneity in melanoma. *Transl Oncol* 2017;10:956–75.

31 Rabbie R, Ansari-Pour N, Cast O, *et al*. Multi-site clonality analysis uncovers pervasive heterogeneity across melanoma metastases. *Nat Commun* 2020;11:4306.

32 Ramón Y Cajal S, Sesé M, Capdevila C, *et al*. Clinical implications of intratumor heterogeneity: challenges and opportunities. *J Mol Med* 2020;98:161–77.

33 Queirolo P, Spagnolo F. Atypical responses in patients with advanced melanoma, lung cancer, renal-cell carcinoma and other solid tumors treated with anti-PD-1 drugs: a systematic review. *Cancer Treat Rev* 2017;59:71–8.

34 Wheen P, Armstrong R, Daly CA. Recent advances in T1 and T2 mapping in the assessment of fulminant myocarditis by cardiac magnetic resonance. *Curr Cardiol Rep* 2020;22:47.

35 Schiza A, Irenaeus S, Ortiz-Nieto F, *et al*. Evaluation of diffusion-weighted MRI and FDG-PET/CT to assess response to AdCD40L treatment in metastatic melanoma patients. *Sci Rep* 2019;9:18069.

36 Reuben A, Spencer CN, Prieto PA, *et al*. Genomic and immune heterogeneity are associated with differential responses to therapy in melanoma. *NPJ Genom Med* 2017;2:10.

37 Klein D. The tumor vascular endothelium as decision maker in cancer therapy. *Front Oncol* 2018;8:367.

38 Gaustad J-V, Simonsen TG, Smistad R, *et al*. Early effects of low dose bevacizumab treatment assessed by magnetic resonance imaging. *BMC Cancer* 2015;15:900.

Supplemental material

BMJ Publishing Group Limited (BMJ) disclaims all liability and responsibility arising from any reliance
placed on this supplemental material which has been supplied by the author(s)

J Immunother Cancer

Supplemental Material

Table S1. Patient demographics.

Patient	ECOG	BRAF Status	Treatment	RECIST 1.1 Evaluation of Standard Clinical CT		Body Site(s) Imaged	No. of Target Lesions Imaged	Research MRI Scan Completion		
				12 Weeks	1 Year			Baseline	3-Weeks	12-Weeks
P1	1	WT	Pembrolizumab	PD	* PD	Subcutaneous	2	Yes	Yes	Yes
P2	1	WT	Pembrolizumab	SD	* PD	Liver	1	Yes	Withdrew from study (claustrophobia and clinical deterioration)	
P3	0	V600 Mutant	Pembrolizumab	PR	PR	Inguinal and external iliac nodes	2	Yes	Yes	Yes
P4	1	WT	Nivolumab	SD	CR	Subcutaneous	4	Yes	Yes	Yes
P5	1	WT	Nivolumab	PD	* PD	Right occipital and posterior cervical region in the neck	1	Yes	Withdrew from study (disease progression)	
P6	1	WT	Pembrolizumab	PD	* PD	Lower limb	1	Yes	Yes	Withdrew from study (disease progression)
P7	0	WT	Pembrolizumab	SD	* PD	Inguinal and external iliac nodes	2	Yes	Yes	Yes

P8	0	WT	Pembrolizumab	PD	PD	Subcarinal/Paraesophageal nodes	2	Yes	Yes	Yes
P9	0	WT	Combined Ipilimumab and Nivolumab	PR	CR	Cervical lymph node and supraclavicular	2	Yes	Yes	Yes
P10	0	WT	Combined Ipilimumab and Nivolumab	PR	CR	Subcutaneous	2	Yes	Yes	Yes
P11	0	V600 Mutant	Combined Ipilimumab and Nivolumab	PD	* PD	Medial clavicle	1	Yes	Withdrew from study (operation and disease progression)	
P12	0	WT	Combined Ipilimumab and Nivolumab	PR	PR	Liver	1	Yes	Yes	Yes
P13	0	WT	Combined Ipilimumab and Nivolumab	PR	PR	Adrenal and liver	1	Yes	Yes	Yes
P14	0	V600 Mutant	Combined Ipilimumab and Nivolumab	SD	PR	Peritoneal and mesenteric nodes	3	Yes	Yes	Yes
P15	1	WT	Combined Ipilimumab and Nivolumab	PD	* PD	Inguinal and iliac nodes	2	Yes	Yes	Study halted due to COVID-19 crisis from March 2020

ECOG = Eastern Cooperative Oncology Group. Treatment response was evaluated based on the Response Evaluation Criteria in Solid Tumors (RECIST) guidelines version 1.1 i.e. Complete Response (CR); Partial Response (PR); Stable Disease (SD); Progressive Disease (PD)

* Represents trial patients who died following disease progression within the first 1 year of follow-up.

Supplemental material

BMJ Publishing Group Limited (BMJ) disclaims all liability and responsibility arising from any reliance placed on this supplemental material which has been supplied by the author(s)

J Immunother Cancer

Table S2. MRI sequence parameters.

Parameter	T_2W	DKI	DCE
Sequence	SSFSE	2D DW EPI	3D FSPGR
TR (ms)	1073-3231	4000-6667	3.2-3.3
TE (ms)	87.6-90.6	92.3-95.3	1.2-1.3
Flip angle (º)	90	90	16
Slice thickness (mm)	6	6	5
Slice gap (mm)	0	0	0
FOV (cm)	28-36	28-36	30-35
Image matrix	256 x 256	128 x 128	160 x 160 x N
Fractional k-space coverage	0.54	1	0.52-0.73
Parallel imaging factor	-	2	2.5
Acquisition time (min)	3:39	11:30	8:07

T_2W = T_2-weighted anatomical scans; DKI = diffusion kurtosis imaging; DCE = dynamic contrast-enhanced MRI; SSFSE = single-shot fast spin-echo; 2D DW EPI = two-dimensional diffusion-weighted echo planar imaging; 3D FSPGR = three-dimensional fast spoiled gradient-recalled echo; TR = repetition time; TE = echo time; FOV = field of view

Figure S1

Supplemental material

BMJ Publishing Group Limited (BMJ) disclaims all liability and responsibility arising from any reliance placed on this supplemental material which has been supplied by the author(s)

J Immunother Cancer
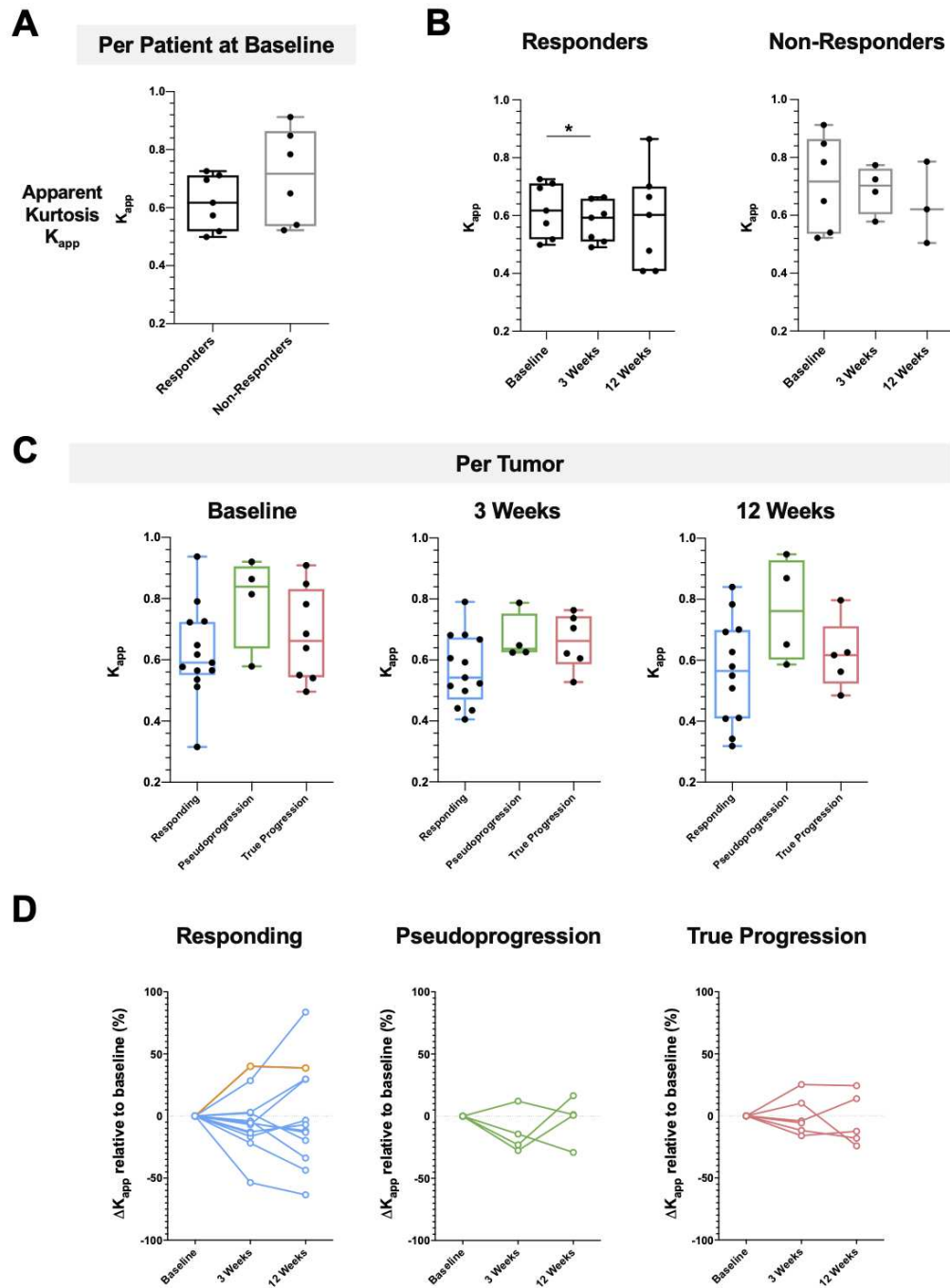
Figure S1

Measurement of tumor heterogeneity using DKI. (**A**) Comparison of apparent kurtosis (K_{app}) as a measure of tumor heterogeneity between responders and non-responders at baseline before the start of treatment. (**B**) Changes in tumor K_{app} among the patients over the course of treatment. (**C**) Differences in tumor heterogeneity among the three subgroups of individual lesions at baseline. (**D**) Percentage change in D_{app} relative to baseline in individual lesions from the three subgroups. * $p < 0.05$. Yellow line in (D) indicates the percentage change in K_{app} for patient P4.

Supplemental material

BMJ Publishing Group Limited (BMJ) disclaims all liability and responsibility arising from any reliance placed on this supplemental material which has been supplied by the author(s)

J Immunother Cancer
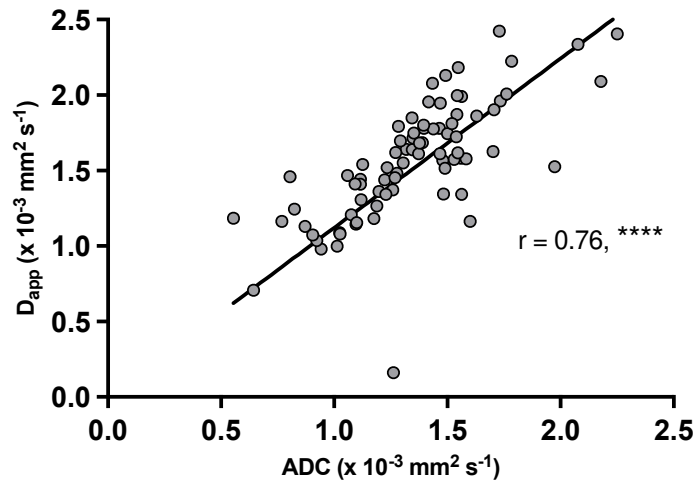
Figure S2

Spearman's correlation analysis showed a positive correlation between the apparent diffusivity value D_{app} measured on DKI and apparent diffusion coefficient ADC measured on DWI. **** $p < 0.0001$.

Figure S3
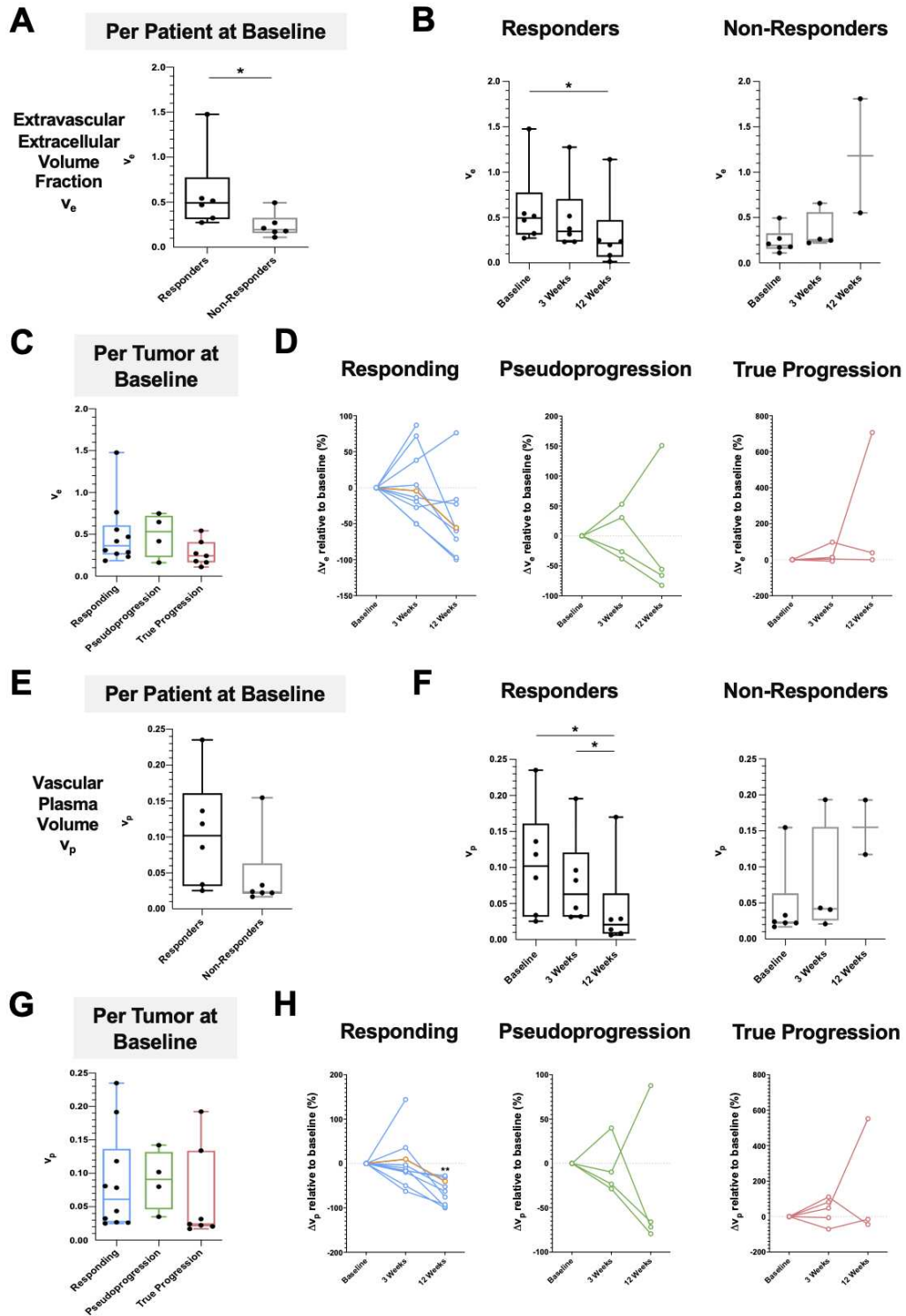
Comparison of changes in DCE-MRI parameters following treatment with immune checkpoint inhibitors among patients and within individual lesions: v_e, extravascular extracellular volume fraction (A-D); and v_p, vascular plasma volume (E-H). * $p < 0.05$; ** $p < 0.01$. Yellow line in (D) and (H) indicates the percentage change in v_e and v_p for patient P4.

Supplemental material

BMJ Publishing Group Limited (BMJ) disclaims all liability and responsibility arising from any reliance placed on this supplemental material which has been supplied by the author(s)

J Immunother Cancer

Figure S4
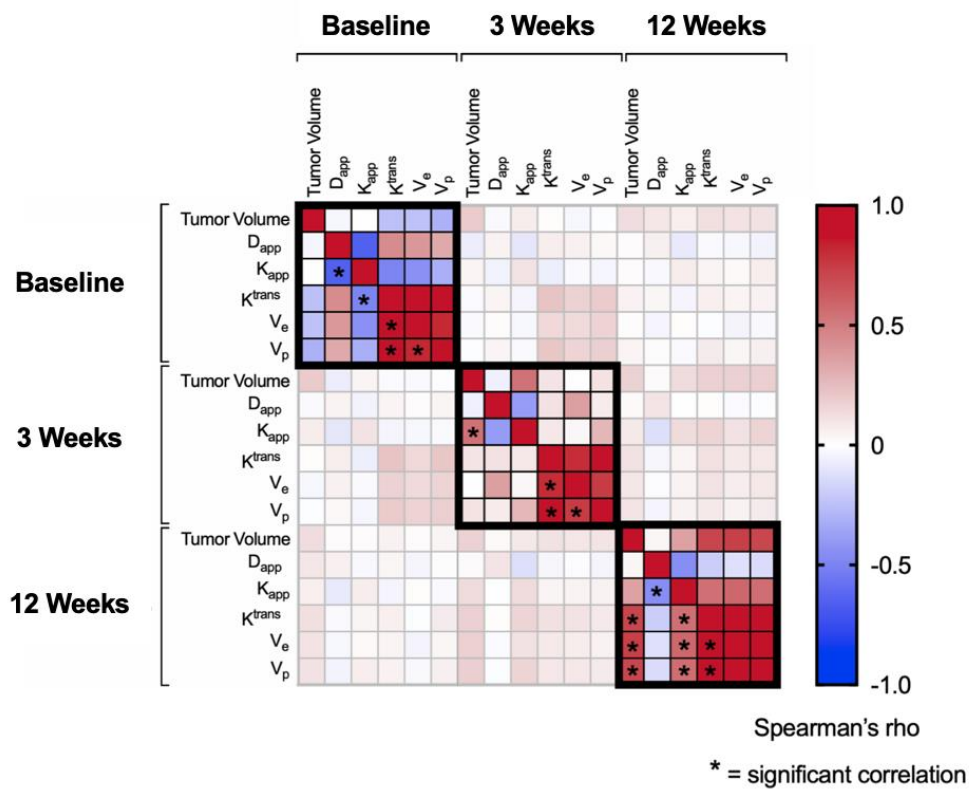
Spearman's correlation analysis of the MRI imaging biomarkers during the first 12 weeks of immune checkpoint blockade.

Supplemental material

BMJ Publishing Group Limited (BMJ) disclaims all liability and responsibility arising from any reliance placed on this supplemental material which has been supplied by the author(s)

J Immunother Cancer

Supplemental Methods

MRI Image Acquisition

T_2-weighted SSFSE images were acquired in coronal, axial, and sagittal orientations (TE/TR = 90.6/1508 ms; slice thickness/gap 6.0/0.0 mm; matrix 256 x 256, NEX 0.54). Axial DKI was acquired using dual-echo EPI (TE/TR = 92.3/6000 ms; slice thickness/gap 6.0/0.0 mm; matrix 128 x 128) with five different b-values (100, 500, 900, 1300 and 1700 s/mm^2). A b-value of 0 s/mm^2 was collected but not used as low b-values have been reported to be susceptible to pseudo-perfusion bias that can be avoided using b-value >100 s/mm^2. Standard diffusion-weighted imaging (DWI) was performed using b-values of 100, 500, 900 s/mm^2. DCE-MRI was performed using a three-dimensional segmented k-space spoiled gradient-echo (3D SPGR) technique in a sagittal orientation. Dynamic phases were acquired at a temporal resolution of 12 s, which included approximately 7 s of scanning and a 5 s gap. The subjects were trained to hold their breath during the gradient noise and to breathe in and out during the periods of silence (TR/TE = 1.2/3.2 ms; flip angle 16°; slice thickness/gap 5.0/0.0 mm; matrix 160 x 160 x number of slices). A bolus injection of the intravascular contrast agent Gadobutrol (Gadovist, Bayer Pharma AG, Berlin, Germany) was administered at 0.1 mmol/kg intravenously 25 s after the start of acquisition at a rate of 3 ml/s, followed by 25 ml of saline flush using an MR-compatible power injector. Pre-contrast T_1-weighted gradient-echo images were acquired with five different flip angles (2°, 3°, 5°, 10°, 15°) and Bloch-Siegert B_1 maps[1] were obtained for subsequent B_1 inhomogeneity correction and T_1 mapping for analysis of the dynamic sequences.

Image Processing and Analysis

Quantitative maps of D_{app} were calculated from the DKI images using an in-house Matlab Script (Mathworks, MA, USA). Non-Gaussian water movements were quantified using a dimensionless metric termed kurtosis, governed by the polynomial equation (**Equation 1**):

$$S_i = S_0 \cdot \exp\left(-b_i \cdot D_{app}\right) \cdot \exp\left(\frac{1}{6} \cdot b_i^2 \cdot D_{app}^2 \cdot K_{app}\right) \tag{1}$$

where s_i is the signal intensity at b-value b_i, s_0 is the estimated signal intensity at *b*-value $b_i = 0$ s/mm^2 when no diffusion gradient is applied, D_{app} is the apparent diffusivity (s/mm^2) at *b*-values more than 1000 s/mm^2, and K_{app} is the apparent diffusion kurtosis (unitless)[2,3].

Quantitative maps of tumor vascular permeability and perfusion were calculated from the DCE images using MISTAR software (Apollo Medical Imaging Technology, Melbourne, Australia). B$_1$ maps of field inhomogeneity were calculated using in-house Matlab scripts for subsequent B$_1$-correction of pre-contrast T$_1$ maps. A model arterial input function (AIF) based on Fritz-Hansen *et al.*[4] and the extended Tofts model [5,6] were used for pharmacokinetic modelling of the intravascular contrast enhancement within tissues. The Fritz-Hansen model AIF was used with values after the first pass extrapolated from the Weinmann function [7], scaled accordingly. Total tissue contrast concentration as a function of time $[C_e(t)]$ can be approximated using (**Equation 2**):

$$C_e(t) = v_p C_p(t) + K^{trans} \int_0^t C_p(t) \, e^{-k_{eP}(t-\tau)} \, d\tau \tag{2}$$

Supplemental material

BMJ Publishing Group Limited (BMJ) disclaims all liability and responsibility arising from any reliance placed on this supplemental material which has been supplied by the author(s)

J Immunother Cancer

where $C_p(t)$ is the concentration in blood plasma as a function of time as determined by the AIF measured in a large feeding vessel, K^{trans} is the volume transfer coefficient from the blood plasma space into the extravascular tumor interstitial space reflecting vascular permeability, v_p is the vascular plasma volume, v_e is the fractional volume of the extravascular-extracellular space, and k_{ep} is the flux rate constant These parameters are interrelated as follows:

$$K^{trans} = v_e \times k_{ep} \qquad (3)$$

Motion correction was performed on all images using in-house Matlab scripts prior to the calculation of quantitative maps.

Volumetric tumor regions of interest (VOIs) were drawn on the T_2-weighted images and quantitative maps of D_{app}, K_{app}, K^{trans} v_e and v_p by a radiologist (FS) with 3 years of experience in the oncological setting and blinded to the clinical outcome and a radiology researcher (DL) with 4 years of experience in oncological imaging. VOIs from each tumor were expressed as single T_2 volume, D_{app}, K_{app}, K^{trans} v_e and v_p values and volume-weighted for analysis for the patient as a whole or for individual lesion. T_2-weighted images taken at each imaging timepoints were normalized based on intensity scaling to the baseline images before calculating the T_2 histograms[8].

Immunohistochemistry

All immunochemistry (IHC) procedures were performed on histologically confirmed melanoma tissues obtained for diagnosis. Tissues were fixed with 10% buffered formalin solution and processed into paraffin embedded (FFPE) tissue blocks. Serial tissue sections of

3.5 µm thickness were prepared from the FFPE blocks and mounted onto silanized slides at Addenbrooke's Hospital Human Research Tissue Bank. IHC and semi-automated image analysis were carried out at AstraZeneca UK. Slides were baked for 1 h at 60°C, deparaffinized in xylene and rehydrated with decreasing concentrations of ethanol. Automated H&E staining was performed on Leica ST5020 Multistainer (Leica Biosystems, Germany). Immunostaining for CD31, Ki67, CAIX, CD8, FOXP3 and CD11b was conducted on a Ventana Benchmark ULTRA automated slide processing system (Ventana Medical Systems Inc., Roche Tissue Diagnostics, Germany) according to the manufacturer's instructions. Briefly, heat-induced epitope retrieval in Tris-EDTA buffer pH 7.8 at 95°C for 44 min was carried out on all slides using Ventana's ULTRA Cell Conditioning 1 (CC1) solution, and endogenous peroxidase activity was quenched using DISCOVERY Inhibitor (Roche Tissue Diagnostics, Germany) at 37°C for 4 min. Primary antibodies incubation was conducted at 37°C for 1 h using the following monoclonal anti-human antibodies: mouse anti-human CD31 (1 µg/ml, clone JC70A, Dako, Denmark), CONFIRM^{TM} rabbit anti-human Ki67 (2 µg/ml, clone 30-9, Roche Tissue Diagnostics, Germany), rabbit anti-human carbonic anhydrase IX (CAIX) (2 µg/ml, clone EP161, Roche Tissue Diagnostics, Germany), rabbit anti-human CD8 (0.58 µg/ml, clone SP239, Spring Bioscience, USA), rabbit anti-human Foxp3 (0.20 µg/ml, clone SP97, Spring Bioscience, USA) and rabbit anti-human CD11b (0.03 µg/ml, clone D6X1N, Cell Signaling Technology, USA). This was followed by secondary antibodies incubation at 37°C for 16 min using either DISCOVERY^{TM} high quality horseradish peroxidase (HQ-HRP) kit for highest sensitivity and specificity in detection and chromogen staining using EnVision FLEX HRP Magenta Substrate Chromogen System (Dako, Denmark), DISCOVERY^{TM} Purple HRP-activated Chromogen kit or DISCOVERY^{TM} Teal HRP-activated Chromogen kits (Roche Tissue Diagnostics, Germany). Human tonsil, spleen and placenta were used as positive control tissues. Immunostaining with mouse or

Supplemental material

BMJ Publishing Group Limited (BMJ) disclaims all liability and responsibility arising from any reliance placed on this supplemental material which has been supplied by the author(s)

J Immunother Cancer

rabbit negative isotype control antibodies (Roche Tissue Diagnostics, Germany) was used as negative controls. Slides were then counterstained with hematoxylin. All stained slides were scanned at 20X and 40X magnification on Aperio AT2 (Leica Biosystems, Germany). Semi-automated image analysis of the whole tissue slides was performed on HALO® software (Indica Labs, USA).

Supplemental material

BMJ Publishing Group Limited (BMJ) disclaims all liability and responsibility arising from any reliance placed on this supplemental material which has been supplied by the author(s)

J Immunother Cancer

References

1. Sacolick LI, Wiesinger F, Hancu I, Vogel MW. B 1 mapping by Bloch-Siegert shift. Magn Reson Med. 2010;63(5):1315–22.

2. Deen SS, Priest AN, McLean MA, Gill AB, Brodie C, Crawford R, et al. Diffusion kurtosis MRI as a predictive biomarker of response to neoadjuvant chemotherapy in high grade serous ovarian cancer. Sci Rep. 2019;9(1):1–9.

3. Goodburn RJ, Barrett T, Patterson I, Gallagher FA, Lawrence EM, Gnanapragasam VJ, et al. Removing rician bias in diffusional kurtosis of the prostate using real-data reconstruction. Magn Reson Med. 2020 Jun 18;83(6):2243–52.

4. Fritz-Hansen T, Rostrup E, Larsson HBW, Søndergaard L, Ring P, Henriksen O. Measurement of the arterial concentration of Gd-DTPA using MRI: A step toward quantitative perfusion imaging. Magn Reson Med. 1996;36(2):225–31.

5. Tofts PS. Modeling tracer kinetics in dynamic Gd-DTPA MR imaging. J Magn Reson Imaging. 1997;7(1):91–101.

6. Paul ST, Gunnar B, David LB, Jeffrey LE, Elizabeth H, Michael VK, et al. Estimating kinetic parameters from dynamic contrast-enhanced t1-weighted MRI of a diffusable tracer: Standardized quantities and symbols. J Magn Reson Imaging. 1999;10(3):223–32.

7. Weinmann HJ, Laniado M, Mützel W. Pharmacokinetics of GdDTPA/dimeglumine after intravenous injection into healthy volunteers. Physiol Chem Phys Med NMR. 1984;16(2):167–72.

8. Sun X, Shi L, Luo Y, Yang W, Li H, Liang P, et al. Histogram-based normalization technique on human brain magnetic resonance images from different acquisitions. Biomed Eng Online. 2015 Dec 28;14(1):73.